Angular Measurements and Analysis of the Indoor Propagation Channel at 60 GHz

Marwan El Hajj, Ghais El Zein, Gheorghe Zaharia, Hanna Farhat, Sawsan Sadek

Angular Measurements and Analysis of the Indoor Propagation Channel at 60 GHz

Marwan El Hajj*, Ghais El Zein*, Gheorghe Zaharia*, Hanna Farhat† and Sawsan Sadek†
* Univ Rennes, INSA Rennes, CNRS, IETR, UMR 6164, F 35000, Rennes, France
† Lebanese University, Faculty of Technology, Saida, Lebanon
Marwan.el-hajj@insa-rennes.fr

***Abstract*—In this work, we present a propagation measurements campaign conducted at 60 GHz in a typical indoor office environment. These measurements can be useful in order to exploit multipaths, aiming to maintain the quality of the communication in the case of blocking the direct path due to an obstruction created by people, furniture or other obstacles. The measurements were realized on 2 GHz bandwidth using a vector network analyzer (VNA). At the receiving side being always visible by the transmitter, a rotation by 6° over 360° is performed. The obtained results allow to compute different channel parameters such as: path loss, RMS delay spread and coherence bandwidth. In our study, we consider for each receiver position two situations: the direct orientation and the best indirect orientation of the receiving antenna. These results show that the path loss of the best indirect orientation increases up to 18 dB compared to the direct orientation. Indeed, some positions may be more affected than others in the case of blocking the direct orientation. The obtained results will be useful both to design the new broadband communication systems and to deploy wireless local and personal area networks (WLAN/WPAN) operating in the millimeter-wave (mmWave) bands.**

***Index Terms*—60 GHz, indoor radio channel, measurements, VNA, path loss, RMS delay spread, coherence bandwidth, angle of arrival**

I. Introduction

Frequency bands already allocated below 6 GHz are no longer sufficient to meet the demand in terms of network capacity. In 5G technology, millimeter-wave frequencies centered at 60 GHz are expected to meet the growing needs imposed by the rise of smart phones and promise high data rates, reliable connectivity and low latency.

Currently, an extensive amount of research is studying mmWave properties in order to deploy future wireless local and personal area networks (WLAN/WPAN) [1]. Many studies have focused on the large-scale propagation characteristics of mmWave bands in order to propose channel models, simulators and new engineering rules for the design of communication systems [2] [3]. The mmWave radio links have high propagation losses and are very sensitive to blockages that cause significant variations in the channel depending on the type of obstacle (furniture, people, walls, etc.) and its relative position [4]. Measurements presented in [5] showed that the human blockage causes attenuation greater than 20 dB and the shadowing effect depends more on the antennas configurations than the number of persons. The human body can damage the direct path between the transmitter and receiver especially when directive antennas are used. To overcome the strong attenuation at 60 GHz, some techniques were proposed. Experimentally, in [6], the path gain can be enhanced by 10 dB to 15 dB by increasing the elevation angles of incidence for near-body user equipments, which provide better performance and indicates that the access point should be placed at larger height. In [7] the authors proposed multiple access points (APs) at 60 GHz and formulated the selection of APs as a Partially Observed Markov Decision Process (POMDP) which avoids 90% of the blockage; even if both APs suffer from the same level of blockage. Other solutions have been proposed using beamforming or beam steering which are able to redirect the beam's path in the ultimate direction regarding the link budget [8]. Analysis based on measurements will be required to better characterize the 60 GHz propagation conditions at specific sites, as it is well known that general channel models can deviate substantially from the conditions experienced by a particular deployment such as in the industrial environments. Measurements at 60 GHz in different indoor environment types such as typical residential [9], conference rooms and hallway have been studied [10] [11]. Based on the previous studies [9-11], we investigate in this paper a specific indoor environment: the open-space office.

The present study is a part of the FUI OptimiSME project, aiming to optimize the deployment of multi-band radio networks for small enterprises. After studying the 2.4 and 5.8 GHz radio propagation in an L-shape open-space indoor office [12], this study focuses on 60 GHz propagation in the same environment by considering different configurations. The goal is to assess indirect propagation path level that could be exploited by systems using smart antennas or beamforming in obstructed configurations.

The paper is organized as follows: Section II describes the measurement set-up and the measurement environment scenario. Section III presents the measurement results and analysis. Finally, Section IV sums up several conclusions.

II. Measurement Set-Up and Scenario

A. Measurement Set-Up

The measurement system presented in Fig. 1 uses a VNA that measures the S_{21} (magnitude and phase) parameter over 401 equidistant sub-carriers sequentially, with 5 MHz frequency spacing. Hence, a 2 GHz bandwidth (based on IEEE 802.11ad standard) [13] is considered, which corresponds to

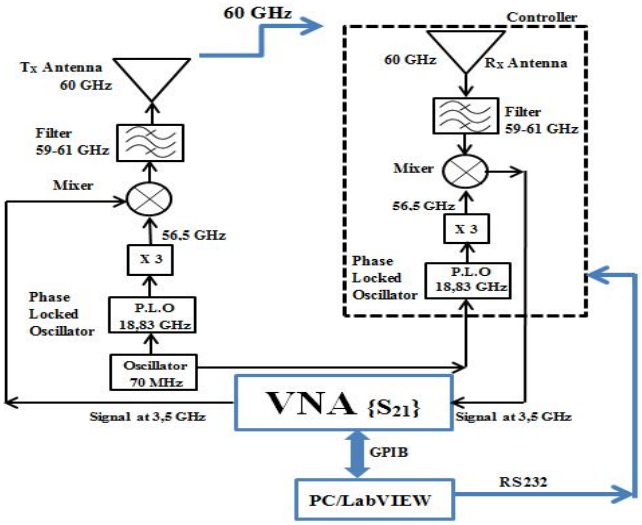

Fig. 1. Measurement system using 60 GHz up and down converters.

0.5 ns of time delay resolution, with the center frequency of 3.5 GHz. The extension to 60 GHz is provided by radio frequency modules (up and down converters) using standard components such as multipliers and mixers. The frequency band of the measurement system is 59-61 GHz. It is imposed by the filter at the transmitter and receiver side as shown in Fig. 1. For the transmitter (Tx), acting as an access point (AP), we used a horn antenna having 100° beam width at -6 dB in both E and H planes (Orange Labs conception) and 7.3 dBi gain. At the receiver (Rx) side, acting as user-equipment, a 22.5 dBi gain horn antenna (QuinStar Technology QWH-1500 -AA) was used with 10° and 13° HPBW (Half Power Beam Width) in E and H planes respectively. The small beamwidth Rx antenna provides excellent spatial resolution, allowing the measurement of multipath arrival angles. Both antennas are vertically polarized and operating between 58 and 62 GHz. The transmitted power at 60 GHz is 0 dBm. Coaxial cables of 1 m and 20 m lengths are used to connect to the VNA the Rx and Tx respectively. The Tx and Rx are set at heights of 1.9 m and 1.2 m respectively, with respect to the ground. Before starting measurements, a full two ports calibration is made to compensate the cable losses. Then, a back-to-back measurement is performed, in order to remove the influence of the up/down converters from the channel frequency response.

B. Measurement Scenario

As shown in Fig. 2, the measurements were performed within an unoccupied (no employees) L-shaped typical office room, located in the IETR laboratory in Rennes, France. The room is furnished with desks, metallic cupboards, boards and has three wooden doors, as shown in Fig. 3. For each measurement, we placed the receiver on a different desk. We consider 9 different receiver positions, as shown in Fig. 3. On the transmitter side, due to its large beam width, Tx is positioned in the corner of the room to be in direct visibility with the different receiver positions. Its central axis is pointed towards a concrete pole (central dashed line in Fig. 3). Tx and Rx locations for the measurement campaign are also shown in the figure.

For each Rx position, rotations are performed by 6° azimuth step over 360° using a positioner. The choice of the rotation angle depends on the aperture angle of the receiver antenna. For each 6° step, the magnitude and phase of the channel frequency response are collected using a PC that commands the VNA via a GPIB cable, and the positioner via an RS232 cable with a LabVIEW program.

Fig. 2. View of the open-space office.

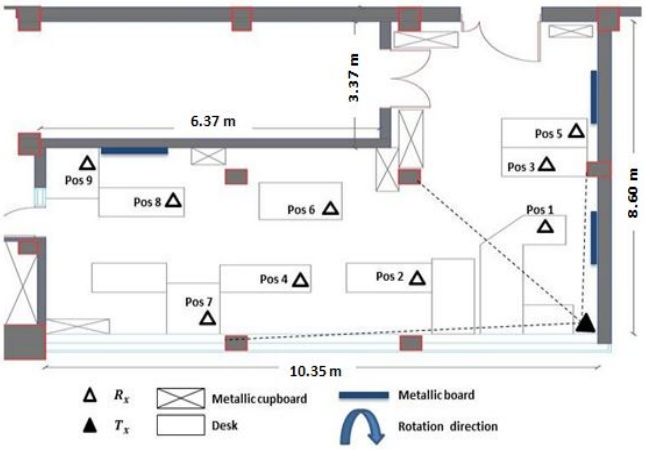

Fig. 3. Top view plan of the open-space office with Rx locations.

III. Measurement Results and Analysis

A. Path Loss

We call direct orientation (DO) the situation when Rx antenna is pointed to the Tx antenna and indirect orientation (IO) otherwise. The best indirect orientation (BIO) corresponds to the highest received power. When analyzing the relative received power for all Rx positions (Fig. 4), we observe the presence of a significant path in the direction of the access point with several reflections depending on the Rx position and rotation angle. Several remarkable reflections are detected, caused by the metallic boards, such as for Pos 9 and Pos 5

and others from surrounding walls and cupboard, such as for Pos 6 and Pos 5.

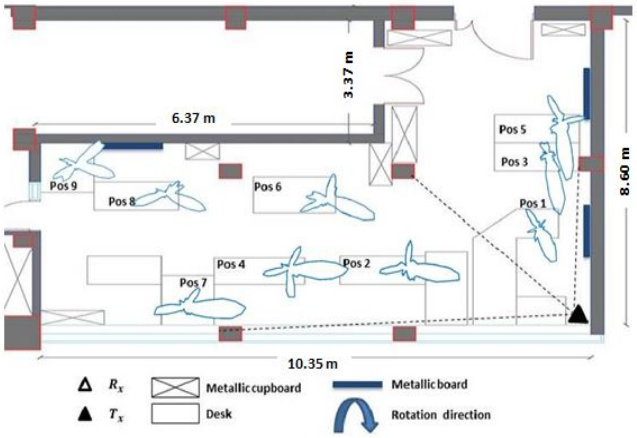

Fig. 4. Top view plan with angular received power at each position.

Fig. 5 illustrates the average path loss (without taking into account the Tx and Rx antenna gains) over the 2 GHz bandwidth for direct and best indirect orientation, function of Rx positions which are numbered from the nearest to the farthest Rx position. The Tx-Rx distance is computed using the x, y and z coordinates of the antennas locations. In general, we remark that the path loss for the best indirect orientation is higher than that for the direct one due to the absence of visibility between the transmitter and receiver antennas. The gap between the DO and the BIO fluctuates between 3.18 dB in Pos 9 and 18.27 dB in Pos 3. For Pos 9, as shown in Fig. 6, the impulse response (computed using the Inverse Fourier Transform IFFT) analysis shows two paths very close to each other. The direct path arrives at 33.4 ns and the best indirect path at 34.57 ns. A difference of 1.17 ns indicates that the best indirect orientation has additional 0.35 m compared to the length of the main path of 10.02 m. Based on the plan of this environment, the location of Pos 9 (Fig. 3) and the Rx angle of the best indirect orientation, we confirm that the second path corresponds to a simple reflection due to the nearest metallic board.

On the other hand, Fig. 7 shows the impulse response of the propagation channel measured at Pos 3 for the direct and best indirect orientations. The impulse response analysis for this position shows very low indirect paths and very delayed with respect to the direct path, due to a multi-reflection, which explains the large variation of path loss in Pos 3. Therefore, in the case of blocking the direct path, this position will receive the lowest power compared to the other receiver positions.

B. RMS Delay Spread

Based on the impulse response for direct and best indirect orientations obtained for the 9 positions, the RMS delay spread defined in [14] was also calculated for each position as follows:

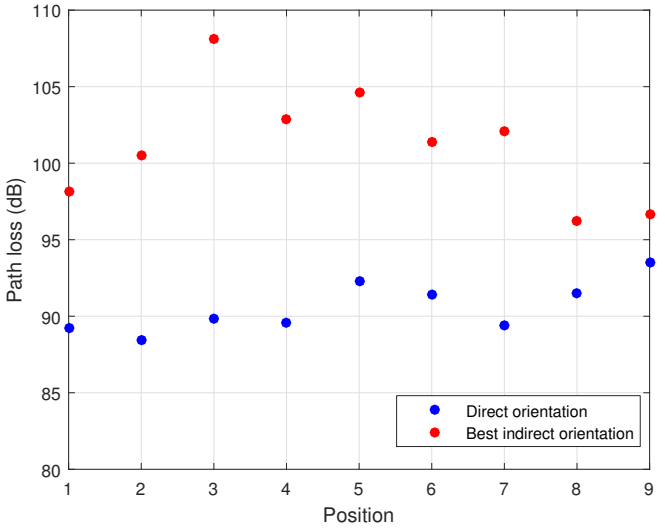

Fig. 5. Path loss for direct and best indirect orientation versus Rx position.

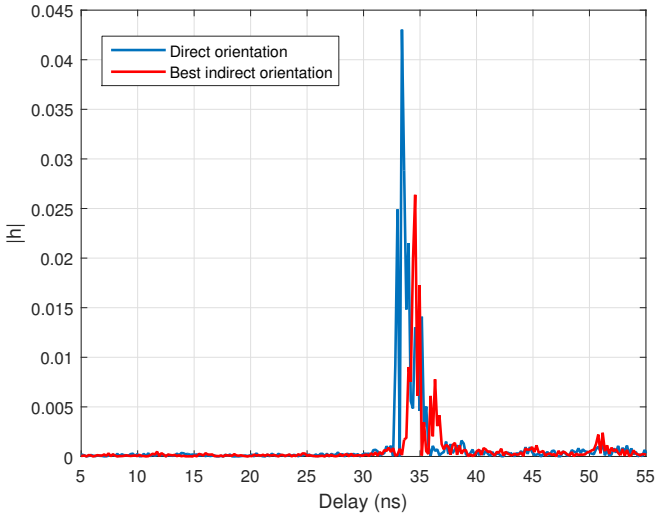

Fig. 6. Impulse response for direct and best indirect orientations for position 9.

$$\tau_{rms} = \sqrt{\bar{\tau^2} - (\bar{\tau})^2} \tag{1}$$

The first moment mean delay is defined as:

$$\bar{\tau} = \frac{\sum_k a_k^2 \tau_k}{\sum_k a_k^2} = \frac{\sum_k P(\tau_k)\tau_k}{\sum_k P(\tau_k)} \tag{2}$$

and, the second moment is defined as:

$$\bar{\tau^2} = \frac{\sum_k a_k^2 \tau_k^2}{\sum_k a_k^2} = \frac{\sum_k P(\tau_k)\tau_k^2}{\sum_k P(\tau_k)} \tag{3}$$

where a_k^2, $P(\tau_k)$ and τ_k are the gain, power and delay of k^{th} path respectively. In order to calculate the RMS delay spread, a threshold of 20 dB dynamic was estimated between the highest level of the impulse response and the noise floor. Moreover, in order to reduce the side lobe level, a Hamming window has been applied in frequency domain. The coefficients of the

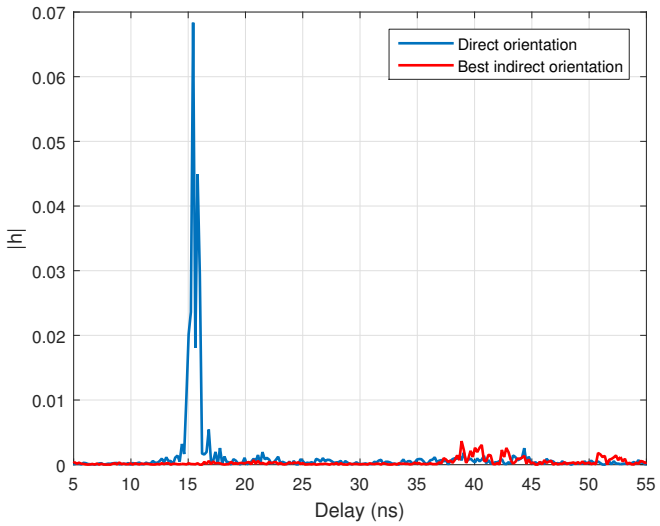

Fig. 7. Impulse response for direct and best indirect orientations at position 3.

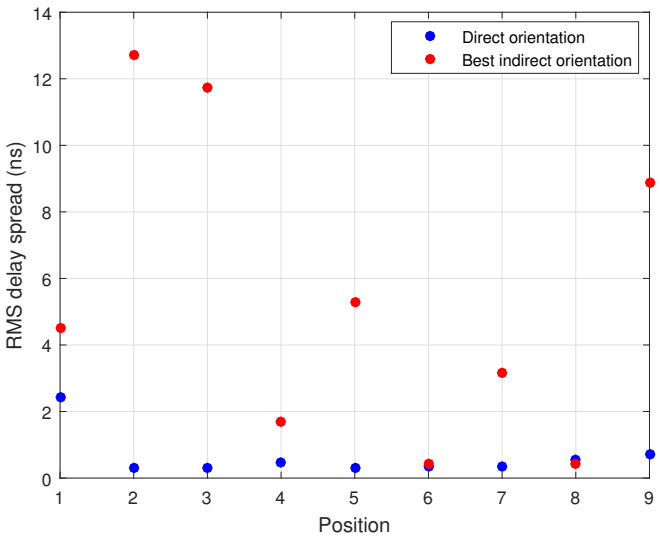

Fig. 8. RMS delay spread variation versus Rx position.

Hamming window are computed from the following relation presented in [15]:

$$w(n) = 0.54 - 0.46cos(2\pi\frac{n}{N}) \quad (4)$$

where N = 401 is the number of the samples used by the VNA for a measurement and n = 0, 1, 2 ,..., N-1. Fig. 8 depicts the RMS delay spread as a function of each Rx position. Overall, Fig. 8 shows that the direct orientation has smaller RMS delay spread than the best indirect one due to the propagation phenomena (reflection, diffraction), except for Pos 6 and Pos 8 which show close RMS delay spread values for both cases. The analysis of the impulse responses obtained at Pos 8 (Fig. 9) shows that the energy is focused around the direct orientation at 27.73 ns and around the best indirect orientation at 42.58 ns. A difference of 14.85 ns between direct and best indirect orientations corresponds to a difference of 4.45 m between the lengths of these paths. Referring to the angular received power (Fig. 10) and using simple geometric calculation relying on image theory, we can find the origin of this specular reflection, which is due to the wooden door nearest to the Pos 8.

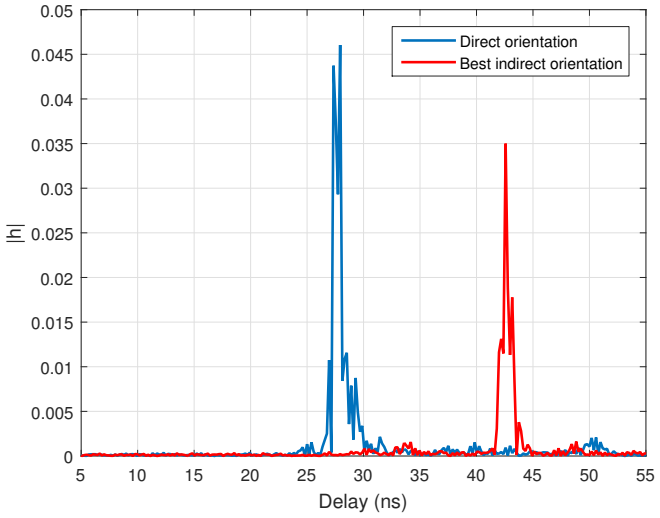

Fig. 9. Impulse response for direct and best indirect paths at position 8.

C. Coherence Bandwidth

Relying on the frequency response of direct and best indirect orientations, the coherence bandwidth (Bc) at -3 dB has been calculated using the complex auto-correlation function [14], as follows:

$$R(\Delta f) = \int_{-\infty}^{+\infty} H(f)H^*(f+\Delta f)df \quad (5)$$

where $H(f)$ is the complex frequency response of the channel, Δf is the frequency shift and * denotes the complex conjugate. The absolute value of $R(\Delta f)$ corresponds to the magnitude of correlation between the channel response at two spaced frequencies. Fig. 11 represents the coherence bandwidth at -3 dB function of Rx position. This figure shows that the coherence bandwidth at -3 dB for direct orientation is higher than the value obtained for the best indirect one. For the direct orientation, Bc varies from 226 MHz up to 547 MHz, while for the best indirect one, it varies from 13.5 MHz to 500 MHz. Pos 8 and Pos 9 have Bc values slightly larger for the best indirect orientation than those obtained for the direct one. Pos 8 presents for the best indirect orientation a coherence bandwidth larger with 36 MHz than the coherence bandwidth obtained for the direct one. If we consider the values obtained for the RMS delay spread at Pos 8 (Fig. 8), the direct path has a slightly higher value than the indirect path. The inverse correlation between RMS delay spread and coherence bandwidth has been expected, when RMS delay spread decreases, coherence bandwidth increases.

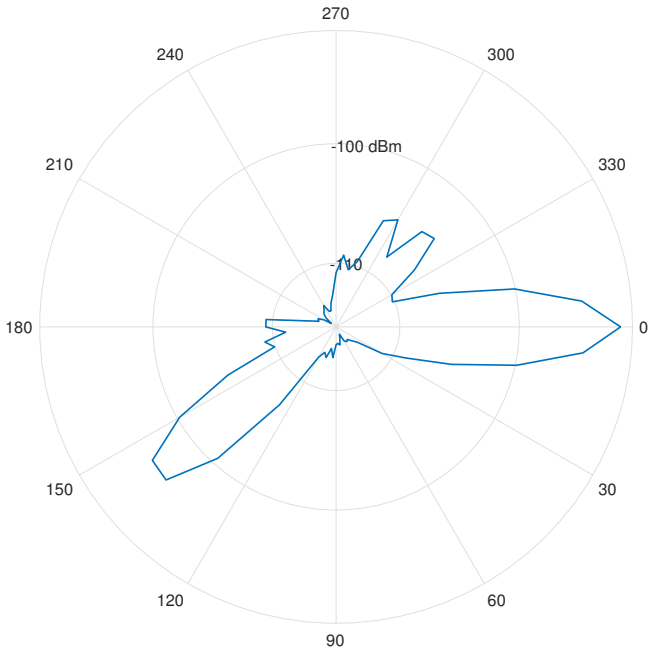

Fig. 10. Angular received power at position 8.

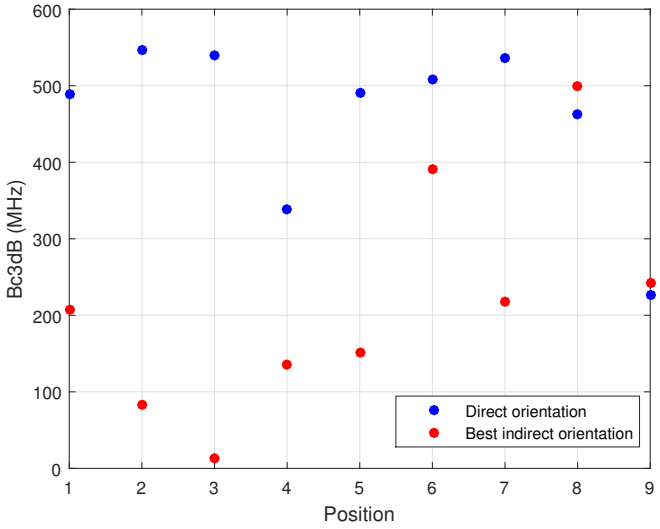

Fig. 11. Coherence bandwidth at -3 dB function of receiver position.

IV. Conclusion

In this paper, the characterization of the radio propagation channel at 60 GHz has been investigated by measurements conducted in a static L-shaped office room. These measurements were used to determine the impulse response of the channel for different receiver positions. For each position, the received angular power has been obteined from a 360° rotation in azimuth plane. We highlight the presence of reflections according to their angles of arrival. For all these positions, the analysis of the obtained channel parameters (path loss, RMS delay spread and coherence bandwidth) was performed by comparing the direct orientation (DO) case of the Rx antenna to the best indirect orientation (BIO) case. These results can be exploited to take advantage of the diversity of multipaths offered by the channel. Thus, when the direct link between transmitter and receiver is obstructed, communication can be maintained, using techniques such as beamforming. Furthermore, dynamic channel measurements for the same indoor scenario are in progress, to asses the effect of people's movement.

Acknowledgement

This work is a part of the French project FUI22 OptimiSME, and the ARED CAMOPROM, and financially supported by Région Bretagne and Rennes Métropole.

References

[1] P. Zhou, K. Cheng, X. Han, X. Fang, Y. Fang, R. He, Y. Long, and Y. Liu, "IEEE 802.11ay-Based mmWave WLANs: Design Challenges and Solutions," *IEEE Communications Surveys Tutorials*, vol. 20, no. 3, pp. 1654–1681, 2018.

[2] S. Sun, G. R. MacCartney, and T. S. Rappaport, "A Novel Millimeter-Wave Channel Simulator and Applications for 5G Wireless Communications," in *IEEE International Conference on Communications (ICC)*, May 2017, pp. 1–7.

[3] 3GPP, "Technical Specification Group Radio Access Network; Study on Channel Model for Frequencies From 0.5 to 100 GHz (Release 14)," in *3rd Generation Partnership Project (3GPP), TR 38.901 V1.0.1*, 2017.

[4] M. Fakharzadeh, J. Ahmadi-Shokouh, B. Biglarbegian, M. R. Nezhad-Ahmadi, and S. Safavi-Naeini, "The Effect of Human Body on Indoor Radio Wave Propagation at 57-64 GHz," in *IEEE Antennas and Propagation Society International Symposium*, June 2009, pp. 1–4.

[5] S. Collonge, G. Zaharia, and G. E. Zein, "Influence of the Human Activity on Wide-Band Characteristics of the 60 GHz Indoor Radio Channel," *IEEE Transactions on Wireless Communications*, vol. 3, no. 6, pp. 2396–2406, Nov. 2004.

[6] L. Zhang, A. McKernan, S. Cotton, and W. Scanlon, "The Influence of Elevation Angle on 60 GHz Near-Body Path Gain," in *12th European Conference on Antennas and Propagation (EuCAP) 2018: Proceedings*. United Kingdom: The Institution of Engineering and Technology, 2018, pp. 1–5.

[7] X. Zhang, S. Zhou, X. Wang, Z. Niu, X. Lin, D. Zhu, and M. Lei, "Improving Network Throughput in 60 GHz WLANs via Multi-AP Diversity," in *IEEE International Conference on Communications (ICC)*, June 2012, pp. 4803–4807.

[8] S. Sun and T. S. Rappaport, "Wideband mmWave Channels: Implications for Design and Implementation of Adaptive Beam Antennas," in *IEEE MTT-S International Microwave Symposium (IMS2014)*, June 2014, pp. 1–4.

[9] M. Kacou, V. Guillet, G. El Zein, and G. Zaharia, "Coverage and Throughput Analysis at 60 GHz for Indoor WLAN with Indirect Paths," in *IEEE 29th Annual International Symposium on Personal, Indoor and Mobile Radio Communications (PIMRC)*, Sept. 2018, pp. 1–5.

[10] V. Semkin, A. Karttunen, J. Jrvelinen, S. Andreev, and Y. Koucheryavy, "Static and Dynamic Millimeter-Wave Channel Measurements at 60 GHz in a Conference Room," in *12th European Conference on Antennas and Propagation (EuCAP 2018)*, April 2018, pp. 1–5.

[11] M. El Hajj, G. Zaharia, G. EL Zein, H. Farhat, and S. Sadek, "Millimeter-Wave Propagation Measurements at 60 GHz in Indoor Environments," *The 14th International Symposium on Signals, Circuits and Systems (ISSCS)*, 2019.

[12] S. Kaddouri, M. El Hajj, G. Zaharia, and G. El Zein, "Indoor Path Loss Measurements and Modeling in an Open-Space Office at 2.4 GHz and 5.8 GHz in the Presence of People," in *IEEE 29th Annual International Symposium on Personal, Indoor and Mobile Radio Communications (PIMRC)*, 2018, pp. 1–7.

[13] IEEE Computer Society LAN/MAN Standards Committee and others, "IEEE standard for information technology-telecommunications and information exchange between systems-local and metropolitan area networks-specific requirements part 11: Wireless LAN medium access control (MAC) and physical layer (PHY) specifications: Amendment 3: Enhancements for very high throughput in the 60 GHz band," *IEEE Std 802.11*, 2012.

[14] T. S. Rappaport, *Wireless communications: Principles and Practice*. Prentice Hall PTR New Jersey, 1996.

[15] F. J. Harris, "On the Use of Windows for Harmonic Analysis with the Discrete Fourier Transform," *Proceedings of the IEEE*, vol. 66, no. 1, pp. 51–83, Jan 1978.